Published in final edited form as:

Microsc Microanal. 2008 December ; 14(6): 532–548. doi:10.1017/S1431927608080884.

Nonlinear Optical Imaging of Cellular Processes in Breast Cancer

Paolo P. Provenzano[1,2,3], **Kevin W. Eliceiri**[2,★], **Long Yan**[2], **Aude Ada-Nguema**[1], **Matthew W. Conklin**[1,2,3], **David R. Inman**[1,3], and **Patricia J. Keely**[1,2,3]

[1]Department of Pharmacology, University of Wisconsin, Madison, WI 53706

[2]Laboratory for Optical and Computational Instrumentation, University of Wisconsin, Madison, WI 53706

[3]University of Wisconsin Comprehensive Cancer Center, University of Wisconsin, Madison, WI 53792

Abstract

Nonlinear optical imaging techniques such as multiphoton and second harmonic generation (SHG) microscopy used in conjunction with novel signal analysis techniques such as spectroscopic and fluorescence excited state lifetime detection have begun to be used widely for biological studies. This is largely due to their promise to noninvasively monitor the intracellular processes of a cell together with the cell's interaction with its microenvironment. Compared to other optical methods these modalities provide superior depth penetration and viability and have the additional advantage in that they are compatible technologies that can be applied simultaneously. Therefore, application of these nonlinear optical approaches to the study of breast cancer holds particular promise as these techniques can be used to image exogeneous fluorophores such as green fluorescent protein as well as intrinsic signals such as SHG from collagen and endogenous fluorescence from nicotinamide adenine dinucleotide or flavin adenine dinucleotide. In this article the application of multiphoton excitation, SHG, and fluorescence lifetime imaging microscopy to relevant issues regarding the tumor-stromal interaction, cellular metabolism, and cell signaling in breast cancer is described. Furthermore, the ability to record and monitor the intrinsic fluorescence and SHG signals provides a unique tool for researchers to understand key events in cancer progression in its natural context.

Keywords

multiphoton excitation microscopy; second harmonic generation (SHG); fluorescence lifetime imaging microscopy (FLIM); spectral lifetime imaging microscopy (SLIM); signal transduction; stromal collagen

★*Corresponding author*. eliceiri@wisc.edu.

INTRODUCTION

Nonlinear optical imaging techniques such as multiphoton excitation microscopy (MPE), second harmonic generation (SHG), used in conjunction with fluorescence lifetime imaging microscopy (FLIM) provide powerful tools to image cellular processes both *in vitro* and *in vivo* (Denk et al., 1990; Brown et al., 2001, 2003; Campagnola et al., 2002; Zoumi et al., 2002; Cox et al., 2003; Eliceiri et al., 2003; Zipfel et al., 2003b; Wang et al., 2005). The purpose of this article is to demonstrate how the application of these three imaging modalities, used in concert to obtain multidimensional data, can help elucidate fundamental issues in breast cancer.

Multiphoton Excitation

Multiphoton laser scanning microscopy (MPLSM) builds upon the advantages brought about by the widespread introduction of confocal laser-scanning microscopy (Brakenhoff et al., 1985; White et al., 1987), which allows thick biological sections to be imaged through optical sectioning. Multiphoton microscopy, first introduced by Denk et al. (1990), is an alternative optical sectioning technique where fluorescence excitation is restricted to the plane of focus, with an effective imaging depth that can greatly exceed conventional confocal microscopy (Denk et al., 1990; Centonze & White, 1998), while better maintaining viability after prolonged exposure to excitation (Squirrell et al., 1999). This is largely due to the fact that multiphoton excitation occurs via multiple low-energy (typically 650–1050 nm excitation) photons acting in concert to produce an emitted photon at the same wavelength as the corresponding single photon excitation, but with less scattering and a nonlinear dependence for fluorescent intensity (Denk et al., 1990; Centonze & White, 1998; Diaspro & Sheppard, 2002; Helmchen & Denk, 2002). Accordingly, for the case of two-photon excitation (TPE), the fluorescence intensity $I_f(t)$ is proportional to the square of the intensity of the laser light $I(t)$ [after (Diaspro & Sheppard, 2002)]:

$$I_f(t) \propto \delta_2 I(t)^2 \propto \delta_2 P(t)^2 \left[\pi \frac{(NA)^2}{hc\lambda}\right]^2, \quad (1)$$

where δ_2 is defined as a molecular cross section that represents the dependence for the probability of TPE on the square of photon density, $P(t)$ is the laser power, NA is the numerical aperture, h is Planck's constant, c is the speed of light, and λ is the wavelength. Therefore, due to this quadratic dependence and the fact that excitation only takes place when multiple low-energy photons are absorbed by a fluorophore, the probability of TPE outside the focal plane is low, resulting in the optical sectioning effect (Denk et al., 1990; Centonze & White, 1998; Diaspro & Sheppard, 2002; Zipfel et al., 2003b), making MPLSM ideal for generating high-resolution images of introduced and/or endogenous fluorophores from deep inside live biological tissues.

Second Harmonic Generation

In contrast to the fluorescent emission resulting from multi-photon excitation, SHG arises from the laser field suffering a nonlinear, second-order polarization when passing through

noncentrosymmetric ordered structures (Freund & Deutsch, 1986; Campagnola et al., 2002; Stoller et al., 2002; Cox et al., 2003; Mohler et al., 2003; Williams et al., 2005; Plotnikov et al., 2006), such as the highly crystalline and hierarchical structure of fibrillar collagen. In general form, this nonlinear polarization can be described as (Stoller et al., 2002; Mohler et al., 2003; Williams et al., 2005):

$$\mathrm{P}=\chi^{(1)}*\mathrm{E}+\chi^{2}*\mathrm{E}*\mathrm{E}+\chi^{(3)}*\mathrm{E}*\mathrm{E}*\mathrm{E}+\ldots, \quad (2)$$

where the polarization (P) and electric field (E) are vectors, and the nonlinear susceptibilities, $\chi^{(i)}$, are tensors. It is the second term in equation (2) that represents SHG. Since SHG is a conserved polarizing process, the resulting coherent wave is exactly half the incident wavelength, with the intensity of the SHG signal proportional to the square of both I and $\chi^{(2)}$ (Shen, 1989; Stoller et al., 2002; Mohler et al., 2003). As such, the SHG signal is proportional to the square laser intensity as well as the molecular concentration (Mohler et al., 2003), organization and orientation (Shen, 1989; Williams et al., 2005) of the sample; allowing the acquisition of information regarding concentration and structure in biological materials. Furthermore, since multi-photon excitation and SHG can be executed simultaneously, yet still be differentiated due to their distinct emission signals, it provides a powerful tool for imaging heterogeneous biological tissues.

Fluorescence Lifetime Imaging Microscopy

Time-domain FLIM is a method to display the spatial distribution of excited state lifetimes (Lakowicz et al., 1992; van Munster & Gadella, 2005), where nonlinear lifetimes (with respect to time) are measured at each pixel and presented as contrast. This fluorescent decay (lifetime) is often well described with the following multiexponential function (Lee et al., 2001; Becker et al., 2004; Bird et al., 2005):

$$I_f(t)=\sum_{i=0}^{n} a_i exp(-t/\tau_i)+c=a_1 exp(-t/\tau_1)+a_2 exp(-t/\tau_2)+a_3 exp(-t/\tau_3)+\cdots+c, \quad (3)$$

where $I_f(t)$ is the fluorescent intensity at some time t following the excitation pulse, n is the number of exponential terms needed to describe the signal well (typically 1 to 3), a is the fractional contribution of each of the components, τ is the fluorescence lifetime, and c is background light noise.

In contrast to fluorescent emission intensity (see equation (1)), the fluorescence lifetime is independent of fluorophore concentration (Lakowicz et al., 1992; Becker et al., 2004; van Munster & Gadella, 2005), providing an additional dimension of information that allows fluorophores to be distinguished or identified. Hence, by combining the advantages of multiphoton imaging discussed above with FLIM to realize multiphoton-FLIM (French et al., 1997; Bird et al., 2005; Parsons et al., 2005), an extra dimension of data can be obtained that can help distinguish or describe processes such as fluorophore and signal identification, molecular activation state, molecular microenvironmental conditions, cellular metabolic

state, protein-protein interactions, and protein-DNA interactions (French et al., 1997; Verveer et al., 2000; Harpur et al., 2001; Tadrous et al., 2003; Bird et al., 2004, 2005; Peter & Ameer-Beg, 2004; Cremazy et al., 2005; Parsons et al., 2005; Peter et al., 2005). Since these processes are highly relevant to breast cancer, the additional information obtained with multiphoton-FLIM is extremely valuable and provides a powerful tool to studying, identifying, and understanding cellular processes both *in vitro* and *in vivo*.

Application of Nonlinear Imaging in Cancer

The capacity to image live tumor cells in their native, as well as engineered, microenvironment significantly enhances our ability to understand cellular behavior and better understand tumor formation, progression, and metastasis. To this end, multiphoton excitation, SHG, and FLIM have all been successfully utilized to better identify, understand, and characterize cancer (Brown et al., 2001, 2003; Jain et al., 2002; Wang et al., 2002, 2004; Palmer et al., 2003; Tadrous et al., 2003; Bird et al., 2005; Parsons et al., 2005; Sahai et al., 2005; Skala et al., 2005). In particular, three-dimensional (3D) imaging of live tissues with MPLSM has been utilized with great success to better understand two fundamental issues in cancer biology *in vivo*, namely, vascular behavior and metastasis (Brown et al., 2001; Jain et al., 2002; Wang et al., 2002, 2005). Employing intravital imaging methodologies, assisted by the introduction of xenograft cells with an engineered fluorophore such as green fluorescent protein (GFP) (Brown et al., 2001; Wang et al., 2002) or multiple fluorophores (Sahai et al., 2005), these researchers have gained insight into single and collective cell behavior *in vivo* (Brown et al., 2001; Wang et al., 2002, 2004) and correlated imaged cell migration and metastasis *in vivo* with gene expression patterns associated with tumor cell invasion and metastasis (Wang et al., 2002, 2004).

In addition to the ability to image exogenous fluorophores, such as GFP, specific biological molecules can be imaged due to their endogenous fluorescence or intrinsic polarization (such as the SHG signal from collagen), allowing examination of native cells and the cell-extracellular matrix (ECM) interaction *in vivo*. Specifically, intrinsic fluorescence from molecules such as nicotinamide adenine dinucleotide (NADH), flavin adenine dinucleotide (FAD), and tryptophan (Patterson et al., 2000; Huang et al., 2002; Zipfel et al., 2003a, 2003b; Kirkpatrick et al., 2005), as well as SHG signals from collagen, muscle, and microtubules (Campagnola et al., 2002; Mohler et al., 2003; Zipfel et al., 2003a, 2003b; Williams et al., 2005; Plotnikov et al., 2006), allow direct *in vivo* imaging of endogenous cells and matrices, in addition to providing noninvasive fluorescent markers for studying metabolism and disease state. For instance, early work by Chance and coworkers (Galeotti et al., 1970) examined NADH in tumor cells, while others correlated changes in NADH intensity and lifetime with metastatic potential (Pradhan et al., 1995) or metabolic changes in response to chemopreventive drugs (Kirkpatrick et al., 2005). Additional work utilizing FLIM on human breast cells further characterized the changes in the lifetime of NADH in live cells in culture (Bird et al., 2005), while separate work employed MPLSM to characterize squamous cell carcinoma *in vivo* largely via tumor associated changes in NADH intensity (Skala et al., 2005), demonstrating the utility of endogenous fluorescence for viewing and studying cancerous cells *in vivo*.

Endogenous signals arising from polarization (i.e., SHG) or time domain studies of endogenous fluorescence (i.e., FLIM) also provide powerful tools for imaging and studying cancer *in vivo*, yet to date have received less attention than multiphoton excitation for imaging live cells within intact 3D tumor microenvironments. One notable exception is the work by Jain and colleagues (Brown et al., 2003), which characterized decreases in collagen in tumors by examining SHG signals after pharmacologic intervention. Furthermore, recent work by our research group utilizing SHG in conjunction with MPE and FLIM has characterized changes in cellular autofluorescence and collagen density in mammary glands and tumors, as well as particular collagen structures, designated tumor-associated collagen signatures, or TACS, associated with live tumor growth and tumor cell invasion (Provenzano et al., 2006). Hence, MPE, SHG, and FLIM are each capable of identifying and characterizing key features of carcinoma *in vivo* and provide robust tools separately, or in conjunction with one another, to elucidate important aspects of cancer biology. Therefore, the purpose of this study is to present data demonstrating how these nonlinear optical imaging techniques can be used to study relevant issues in breast cancer, such as the tumor-stromal interaction, tumor cell metabolism, and cell signaling.

MATERIALS AND METHODS

Cell Culture

T47D cells were obtained from the American Type Culture Collection; MDA-MB-231 cells were a kind gift from Dr. Alan Rapraeger (University of Wisconsin); COS-7 cells were obtained as a generous gift from Dr. Richard Anderson (University of Wisconsin, Madison, WI). In certain experiments MDA-MB-231 or COS-7 were transfected with either EGFP, EGFP-Vinculin, EGFP-R-Ras, EGFP-Cdc42(WT), EGFP-Cdc42(61L), or EGFP-Cdc42(17N) as indicated in the text. EGFP-Vinculin was a kind gift from Dr. Anna Huttenlocher (University of Wisconsin), EGFP-R-Ras was subcloned into the EGFP-C1 vector, and cdc42 constructs were a kind gift from Dr. A.R. Howitz (University of Virginia). T47D cells were cultured at 37°C with 10% CO_2 while being maintained RPMI supplemented with 10% fetal bovine serum and insulin (8 μg/mL). MDA-MB-231 cells were maintained in DMEM supplemented with 10% fetal bovine serum and cultured at 37°C with 10% CO_2. COS-7 cells were maintained in DMEM containing high glucose, L-glutamine, sodium pyruvate, and pyridoxine hydrochloride) plus 10% fetal bovine serum at 37°C with 5% CO_2.

Cells were cultured and imaged under standard two-dimensional (2D) conditions or within 3D collagen matrices. For 3D culture cells were cultured within a 2.0 mg/mL type-I collagen gel (rat-tail collagen solution, BD Biosciences) neutralized with 100 mM HEPES in 2X PBS. Following gel polymerization for 1 h, gels were soaked in cell specific media (described above) and maintained at 37°C with 10% CO_2 until imaged as described in the text.

Mammary Tumors

All animal experiments were approved by the institutional animal use and care committee and meet National Institutes of Health (NIH) guidelines for animal welfare. To generate

mammary tumors, polyoma middle-T (PyVT, also commonly abbreviated PyMT or PyV-MT) mice (Lin et al., 2003) were employed. For MPE, SHG, and FLIM imaging of live unfixed, intact (not sectioned), nonstained PyVT tumors, tumors were harvested and live tissue maintained in buffered media at 37°C. All tissues were imaged immediately following tissue harvest.

Instrumentation

For all microscopy experiments reported herein, two separate custom designed multiphoton systems were employed at the University of Wisconsin LOCI laboratory (Wokosin et al., 2003; Bird et al., 2004, 2005). The first system is a multiphoton laser scanning optical workstation (Wokosin et al., 2003) constructed around a Nikon Eclipse TE300 that facilitates multiphoton excitation, SHG, and FLIM. All SHG imaging was performed on this microscope and was detected from the back-scattered SHG signal (Williams et al., 2005). A 5 W mode-locked Ti:sapphire laser (Spectra-Physics-Millennium/Tsunami) excitation (laser field) source producing around 100 fs pulse widths was tuned to wavelengths between 780 or 900 nm. The beam was focused onto the sample with a Nikon 60X Plan Apo water-immersion lens (N.A. = 1.2). Multiphoton and SHG signals were discriminated with 464 nm (cut-on) long pass and 445 nm narrow band pass filters, while GFP signals were isolated with a 480–550 nm (band-pass) filter (all filters: TFI Technologies, Greenfield, MA). Intensity and FLIM data were collected by a H7422 GaAsP photon counting PMT (Hamamatsu) connected to a time correlated single photon counting system (SPC-730, Becker & Hickl).

The second microscope has been recently described in detail (Bird et al., 2004, 2005) and allows generation of multiphoton excitation intensity images in conjunction with FLIM images. In short, the system is built around an inverted microscope (Diaphot, 200, Nikon, Melville, NY) possessing a Bio-Rad MRC-600 confocal scanning unit (Bio-Rad, Hercules, CA) with source illumination from a Ti:Sapphire mode-locking laser (Coherent Mira, Coherent, Santa Clara, CA) pumped by an 8-W solid-state laser (Coherent Verdi) to generate pulse widths of approximately 120 fs at a repetition rate of 76 MHz, with a tuning range of ~700–1000 nm. The confocal scanning unit produces a focused scanning spot that moves across the focal plane of the imaging objective after which the laser beam is transmitted to the microscope through a transfer lens (01LAO159, Melles Griot, Rochester, NY) and impinges on a dichromatic mirror (650DCSP, Chroma, Inc., Rockingham, VT) that directs incident illumination to the imaging objective (60X oil immersion, 1.4 NA, Nikon) while allowing the emitted visible fluorescent light to be transmitted to a fast photon-counting detector (PMH-100, Becker & Hickl). FLIM images were acquired with an electronic system for recording fast light signals by time correlated single photon counting (SPC-830, Becker & Hickl).

Acquisition for both MPLSM systems was done with WiscScan (Nazir & Eliceiri, 2008), a lab developed software acquisition package that can control both the MPLSM and FLIM collection. Image analysis for combined (and separated) MPE-SHG was performed with ImageJ (Abramoff et al., 2004) and VisBio (Rueden et al., 2004) software. Fluorescent lifetime analysis was carried out with SPCImage (Becker & Hickl), which can fit fluorescent

decay data with the exponential function (equation (3)), for one, two, or three terms, and sum individual photon counts for each pixel to construct a contrast image. The incomplete model approach in SPC Image (ref SPC Image manual) was used to compensate for instances where the fluorescence decay is slow compared to the time window defined by the repetition rate of the laser system.

RESULTS AND DISCUSSION

Relevant Issues in Breast Cancer

It is estimated that one in seven women have a lifetime probability of developing breast cancer and that in the year 2005 approximately 270,000 women will be diagnosed with breast cancer with an overall mortality rate of ~15% and lower survival associated with invasive and metastatic cancer (American Cancer Society annual statistics; www.cancer.org). As such, techniques and tools to detect, characterize, study, and combat breast cancer are of great significance.

One of the largest risk factors for developing breast carcinoma is high breast tissue density (Boyd et al., 2002). Dense breast tissue is linked to a four-to-sixfold increased risk of breast carcinoma (Boyd et al., 1998, 2001), and it is known that high breast density is associated with increased collagen deposition and content (Guo et al., 2001). Therefore understanding epithelial-stromal (-collagen) interactions is of great relevance, and this importance is further highlighted by information that improper stromal-epithelial interactions can promote tumorigenesis (Ronnov-Jessen et al., 1995; Elenbaas et al., 2001; Tlsty & Hein, 2001) and that metastatic breast carcinoma cells migrate away from tumors along collagen fibers (Wang et al., 2002). Moreover, aberrant signal transduction, altered metabolic state, genetic mutations, and altered transcriptional profiles have all been associated with carcinoma formation, progression, and metastasis (Hagios et al., 1998; Hanahan & Weinberg, 2000; Jacks & Weinberg, 2002; Muti, 2004; Rangarajan et al., 2004; Condeelis et al., 2005; West et al., 2005). Therefore, as indicated in the previous section, MPE, SHG, and FLIM (or FRET-FLIM) either individually or in combination are very well suited to address important issues associated with each of these important areas of breast cancer research by utilizing both introduced (i.e., fluorescent probes, fluorescence resonance energy transfer (FRET) probes in FRET-FLIM, etc.) or endogenous (i.e., NADH, collagen etc.) signals. Examples of this utility are illustrated below.

Breast Cancer Related Tumor-Stromal Interactions

Understanding tumor-stromal interactions, both *in vitro* and *in vivo*, is an important aspect of the study of tumor formation and progression since stromal-epithelial interactions play a critical role in both tumorigenesis and metastasis (Ronnov-Jessen et al., 1995; Elenbaas et al., 2001; Tlsty & Hein, 2001; Wang et al., 2002; Sato et al., 2004; West et al., 2005). To help elucidate the mechanisms associated with tumor-stromal interactions in breast cancer, optical imaging modalities that allow deep imaging of live tissue are of great utility. As seen in Figure 1, combined MPE and SHG facilitate viewing of intact live mammary tumor tissue. Figure 1 represents six planes of a 30-plane z-stack (10 μm steps; 300 mm total range), obtained at 890 nm excitation, which clearly shows collagen surrounding and within

the tumor (i.e., SHG signal), as well as endogenous tumor cell fluorescence (i.e., MPE). Importantly, variations in both collagen structure and tumor cell autofluorescence across and within imaging planes can be simultaneously acquired. Additionally, changes in local and global collagen density and specific stromal structures that influence tumor cell behavior can be obtained and defined (Provenzano et al., 2006). Hence, by studying the combined MPE/SHG signals in unfixed, unstained, nonsectioned tissues, the structure and composition of the stroma, as well as the degree and type of endogenous tumor-stromal interaction can be obtained.

To further differentiate signals (i.e., biological components) of the tumor, specific filtering techniques can be employed. By exploiting the fact that MPE excitation obeys the fundamental physical relationship of energy loss after excitation (i. e., emission of a lower energy, longer wavelength, photon following excitation by a higher energy photon) while SHG signals are exactly half of the excitation wavelength, the MPE and SHG signals can be separated (Fig. 2). Following excitation of live mammary tumor tissue at 890 nm (a wavelength that produces endogenous cellular fluorescence and SHG of type I collagen) a 464 nm (cut-on) long pass filter was used to isolate the MPE signal while a 445 nm narrow band pass filter was used to separate the signal resulting from SHG. This approach allows clear visualization of the structure and organization of collagen in the stroma as well as the presence and arrangement of stromal fibroblast-looking cells surrounding less fluorescent epithelial tumor cells (Fig. 2). Stromal cells clearly possess a more mesenchymal phenotype, demonstrate a greater fluorescent intensity, and associate with the collagenous stroma, with cells often aligned with collagen fibers. Thus, the use of combined MPE/SHG has the potential to help identify and differentiate additional features that are either not obtainable or not easily obtained with more traditional fluorescent microscopy techniques. Furthermore, the fact that collagen signals primarily arise from the conserved SHG polarization following high wavelength (i. e., 860–920 nm) excitation, FLIM can be used to image and identify collagen (and other SHG generating proteins), as wells as fluorescent signals from live cells (Fig. 3). Since SHG is a conserved polarization processes, the resulting signal following excitation has a theoretical lifetime of zero (i. e., no lifetime), while fluorescent signals have a lifetime that are fluorophore and microenvironment dependent. For example, mathematical analysis using a one- or two-term exponential model (equation (3)) of 10 locations that appear to be collagen structures in Figure 3 indicate that 99.3 ± 2.3% (a_1) of the lifetime signal (τ_1) is similar to the calibrated instrumental response function, indicating an essentially zero lifetime, signifying the signal results from SHG. In contrast, examination of fluorescent lifetime characteristics of tumor cells in Figure 3 indicates two distinct lifetime components, τ_1 0.243 ± 0.032 and τ_2 2.61 ± 0.292 (n 6 locations; mean ± *SD*) with a fractional ratio a_1:a_2 of 3.99 (Fig. 3c), that represent different fluorescent molecules or different microenvironmental conditions and/or protein association states for the fluorophore (see the Results and Discussion sections on Breast Cell Metabolism and on Imaging Signaling Events Relevant to Breast Cancer). Hence, FLIM allows identification of different proteins by supporting the concept that the majority of collagen signals arise from SHG at the correct excitation, which differs from the endogenous fluorescent signals occurring in live cells. Moreover, we are able to obtain MPE and SHG simultaneously and FLIM

sequentially on the same system, providing powerful multidimensional data to analyze the tumor-stromal interaction in live tissue.

In addition to the powerful data obtained from live tissue imaging with MPE, SHG, and FLIM, significant understanding can be gained by applying these technologies to more controllable *in vitro* systems. For instance, studying breast epithelial cells within reconstituted 3D matrices *in vitro* (Keely et al., 1995; Wozniak et al., 2003) provides a potent and relevant model system for understanding cell behavior *in vivo*, particularly the epithelial-stromal interaction. For instance, studies on breast epithelial cells in 3D have demonstrated that improper regulation of integrin behavior, integrin mediated adhesion to the ECM, and adhesion mediated signaling profoundly influence cell signaling that can result in a more transformed phenotype (Keely et al., 1995; Wozniak et al., 2003; Paszek et al., 2005). Furthermore the physical act of tumor cell invasion and metastasis is largely, but not solely, regulated by integrins and focal adhesion signaling (Friedl & Wolf, 2003; Friedl et al., 2004), with staining for β_1 integrin (a primary collagen receptor) localized at the leading edge of migrated melanoma cells from 3D tumor explants (Hegerfeldt et al., 2002; Friedl et al., 2004). A similar behavior can be seen in live breast carcinoma cells. Inspection of live highly migratory MDA-MB-231 invasive breast carcinoma cells within reconstituted 3D collagen matrices further highlights the cell-matrix interaction via 3D-matrix adhesions (Fig. 4). Simultaneous imaging of GFP-Vinculin with MPE and the collagen gel with SHG reveals vinculin positive 3D-matrix adhesion at the cell-ECM interface. Early morphology of MDA-MB-231(GFP-Vinculin) cells seeded into collagen matrices after 3 h (Fig. 4a–c) indicates that the cells have not fully spread and exhibit vinculin positive filopodia-like structures that interact with collagen fibrils (see Fig. 4c). This early interaction is likely an early step in cell anchorage and spreading, followed by contractility-mediated reorganization of the ECM, and ultimately migration. As such, examination of migratory MDA-MB-231(GFP-vinculin) cells after 24 h in the 3D matrices show aligned collagen fibers associated with vinculin localization (Fig. 4d–f), which are similar to results from melanoma cells in 3D collagen gels *in vitro* (Hegerfeldt et al., 2002; Friedl et al., 2004). Hence, simultaneous imaging of cellular processes and matrix organization and structure with combined MPE/SHG not only facilitates imaging of nonnative and endogenous signals *in vivo*, but also provides a robust tool to study tumor-stromal interactions in live (unfixed, unstained, nonsectioned) cells *in vitro*, which can further our understanding of the *in vivo* condition.

Breast Cell Metabolism

Intrinsic fluorescence allows imaging of cells and tissues in their native environment, often conferring an advantage over imaging an introduced fluorophore when viewing biological structures in a relatively unperturbed environment is desired. Moreover, changes in metabolic status can be indicative of a diseased state (Galeotti et al., 1970; Pradhan et al., 1995; Pitts et al., 2001; Katz et al., 2002; Palmer et al., 2003; Kirkpatrick et al., 2005). For example, differences in NADH have been used to differentiate normal and cancerous epithelial tissues (Skala et al., 2005) with NADH intensity and lifetime altered with metastatic potential (Pradhan et al., 1995); specific metabolic changes in NADH and

tryptophan in response to chemopreventive drugs has been reported (Kirkpatrick et al., 2005).

Since biological tissues are heterogeneous, excitation often results in emission from multiple fluorophores with overlapping spectra. Therefore, understanding the spectral properties of key fluorophores that correlate with specific cellular activity and that utilize specific excitation wavelengths as a tool to image endogenous structures are of great utility. While multiple sources of biological autofluorescence exist (see Ramanujam, 2000; Zipfel et al., 2003a, 2003b), three strong (primary) sources of cellular autofluorescence are NADH (maximum $\lambda_{ex}/\lambda_{em}$: 350/450 nm), FAD (maximum $\lambda_{ex}/\lambda_{em}$: 450/535 nm), and tryptophan (maximum $\lambda_{ex}/\lambda_{em}$: 280/340 nm). Figure 5 illustrates changes in breast tumor cell and matrix fluorescent intensity and localization as a function of excitation wavelength. At λ_{ex} = 780 nm, a wavelength that is close to the ideal two-photon absorption peak of NADH, a reasonably homogeneous pattern of en dogenous cellular fluorescence in the cytoplasm is clearly visible (Fig. 5a). However, as the excitation wavelength is increased in 20 nm increments to 880 nm, changes in fluorescent intensity and localization can be discerned and the emergence of collagen SHG signal at λ_{ex} = 860–880 can be detected (Fig. 5); likely indicating changes in emission transitioning from TPE of NADH to FAD and possibly a relatively small three-photon excitation of tryptophan and/or three-photon excitation of a lower 260 nm peak for NADH.

To study changes in cellular metabolism in a more homogeneous and controllable system, MPE and FLIM can be applied to normal and cancerous breast cells *in vitro*. Previous work in the "normal" MCF10A human breast cell line demonstrated that FLIM is useful to study the reduction/oxidation state of intracellular NADH by determining the ratio of free (τ_1) and protein bound (τ_2) NADH. Importantly, the ratio of free and protein bound NADH correlates to metabolic state and growth conditions (Bird et al., 2005). Figure 6 represents a fluorescence lifetime image of T47D breast carcinoma cells acquired at λ_{ex} = 740 nm in a 2D environment with the color map representing the weighted average of the short and long components of NADH: $\tau_m = (a_1\tau_1 + a_2\tau_2)/(a_1 + a_2)$. The key advantage of utilizing FLIM is that the lifetime is independent of fluorophore (NADH in this case) concentration and clearly demonstrates the ability to image pertinent metabolic conditions in relevant breast carcinoma cells. In addition, FLIM facilitates the imaging and analysis of breast carcinoma cells in model 3D environments (Fig. 7) and live mammary tissue and tumors (see Fig. 3). Figure 7 represents MDA-MB-231 breast carcinoma cells in 3D collagen gels imaged at λ_{ex} = 890 nm. Again the color map represents the weighted average of the two-term model components and validates the ability to detect changes in cellular lifetime in highly invasive breast carcinoma cells. Hence, imaging the cellular fluorescence lifetime combined with MPE/SHG to study cell metabolism in conjunction with tumor-stromal interactions not only provides images of endogenous structure both *in vitro* and *in vivo*, but can also provide a robust tool to study changes in metabolism associated with disease state, complex cell behavior associated with tumor formation and progression, and the response to chemotherapeutic compounds.

Imaging Signaling Events Relevant to Breast Cancer

Aberrant cell signaling events and the signaling pathways associated with changes in cell survival, proliferation, and the transformed phenotype are critical phenomena that need to be elucidated in breast cancer. Although many studies have utilized GFP tagged signaling approaches to better understanding cellular processes with standard fluorescence and confocal microscopy (for example, see Lippincott-Schwartz et al., 2001; Zhang et al., 2002; Lippincott-Schwartz & Patterson, 2003), less work has been performed utilizing MPE of fluorescently-tagged signaling molecules in live cells, particularly utilizing combined MPE and SHG in 3D. However, several works have shown that MPE can be used in live cells to better understand key signaling events and other cellular processes (Strome et al., 2001; Robu et al., 2003; Poteryaev et al., 2005; Squirrell et al., 2006). In Figure 8, MDA-MB-231 was transfected with either GFP, or GFP tagged wild-type (WT), constitutively active (61L), or dominant negative (17N) constructs of cdc42. Live cells within type I collagen gels were imaged with combined MPE/SHG at λ_{ex} = 890 nm to detect changes in cell morphology and tagged-cdc42 localization as well as cell-induced changes in collagen gel microstructure (Fig. 8). After 6 h within 3D collagen gels, cells expressing constitutively active cdc42 (61L) were more spread and formed more cell protrusions than either control GFP cells or cells expressing dominant negative cdc42 (17N) form and have began to align the collagen matrix (Fig. 8a–c). Moreover, cells with active cdc42(61L) had begun to organize and align the collagen matrix with clear cell matrix interactions while cdc42(17N) expressing cells had not (Fig. 8a–c). Of additional note, cells expressing wild-type cdc42 (GFP-cdc42(WT)) possessed long cell protrusions compared to control GFP cells but were not as spread as cdc42(61L) cells (Fig. 8d,e), possibly indicating that these cells overexpress cdc42 compared to control GFP cells, further suggesting that cellular protrusion (filopodia) and cell spreading correlates to the amount of active cdc42. Combined with the early filopodia-matrix interactions at 3 h (Fig. 4), these data may suggest that activated cdc42 (which is known to regulate filopodia protrusion (DeMali & Burridge, 2003; Jaffe & Hall, 2005)) results in increased early matrix interactions resulting in a more spread cell by 6 h. However, additional studies are required to better understand the temporal relation of cell morphology and signaling in 3D environments. Yet, Figure 8 clearly demonstrates the ability of combined MPE/SHG to image relevant signaling events in live breast carcinoma cells and their interaction with, and modulation of, the extracellular matrix.

Hence, recent advances in imaging allow the elucidation of signaling events in live cells with increased spatial and temporal resolution. Temporal studies of molecules tagged with GFP or other chromophores tracked over time are of great significance to understanding fundamental processes in breast cancer. For instance, localization to the plasma membrane is of particular significance for several key signaling molecules that traffic between the cytosol and membrane, such as the Rho GTPases, or within membrane bound endosomal compartments, such as Rab GTPases. Moreover, it is widely believed that the plasma membrane contains subdomains that contain differing lipid compositions, such as lipid microdomains or lipid rafts. However, the successful imaging of these domains has been generally rather elusive, but may be possible through nonlinear optical techniques, such as multiphoton FLIM, which provides information regarding the local microenvironment. We have found that the use of FLIM to monitor the spatial localization of GFP-tagged molecules

has resulted in a novel elucidation of subdomains within sites of plasma membrane localization. For example, use of MPE at 900 nm to image GFP-tagged constitutively active R-Ras, a member of the Ras family of GTPases that is relevant to breast cell behavior (Keely et al., 1999; Wozniak et al., 2005; Ada-Nguema et al., 2006), demonstrates localization of R-Ras to sites of active membrane protrusion (Fig. 9a) in easily manipulated COS-7 cells. However, the same image analyzed and then color mapped for the fluorescent lifetime of the GFP-R-Ras demonstrates distinct domains along the protruding membrane that are not observed with MPLSM alone (Fig. 9b,c). Although we currently do not know whether these subdomains represent lipid microdomains, biochemical data support the partitioning of R-Ras into lipid microdomains (data not shown), suggesting that FLIM could be a useful tool to image and identify these regions in live cells.

Similar results are obtained when imaging fluorescent molecules that intercalate into membranes, such as filipin. Imaging of filipin via confocal microscopy (not shown) or via MPE demonstrates uniform staining of the entire plasma membrane, with no elucidation of additional structure or microdomains (Fig. 10a). However, when the same image is analyzed by FLIM, the presence of two populations of filipin molecules emerges (Fig. 10b). Again, these distinct regions likely represent two physically or biochemically distinct environments, and are consistent with the partitioning of filipin into cholesterol rich regions. Indicating that the use of FLIM has the potential to identify and image additional features within cells that are not apparent with intensity data alone. Consequently, additional studies combining MPE, SHG, and FLIM to better define the nature of key cell signaling events, cell-matrix regulated or regulating signals, and specific plasma membrane subdomains are ongoing.

Hence, using MPLSM to obtain MPE, SHG, and FLIM (or FRET-FLIM) either individually or in combination provides the potential to help elucidate fundamental processes in breast cancer. By utilizing fluorescent probes, endogenous fluorescence, biological protein polarizations, and FRET technologies, in conjunction with standard biochemical and molecular biology techniques, important questions in cancer research can be addressed in a more in depth and unperturbed manner. Thus, the combined utility of the multidimensional information obtained from these imaging modalities when applied to cells and tissues provides a relatively unique view of the relevant biological system that can explain mechanisms of tumor formation and progression.

Future Directions: Instrumentation, Bioinformatics, and Analysis

MPLSM is emerging as a powerful tool to understand breast cancer in cells, animal models, and harvested human tumor tissue. Furthermore recent advances in detector technology hold great promise for improved detection of weakly fluorescent samples and combined detection of dimensions other than intensity such as spectral and lifetime (Bird et al., 2004). For instance, Figure 11 is a spectral lifetime (SLIM), image generated by the authors of H&E stained PyVT mammary tumor sections that clearly demonstrate the ability to measure the fluorescent lifetime of different spectra and separate out noise from adjacent spectra. Hence, these techniques, possibly combined with improved fluorescent probes (Zhang et al., 2002), are being developed for enhanced detection of autofluorescence and exogenous fluorophores, as well as FRET, FRET-FLIM, and FRET-SLIM experimentation.

Furthermore, in conjunction with these advances in microscopy technologies, development of publicly available image visualization and analysis tools such as the Open Microscopy Environment (Eliceiri & Rueden, 2005; Goldberg et al., 2005), VisBio (Rueden et al., 2004), and ImageJ (Abramoff et al., 2004) are critical to provide image informatics infrastructure for the dissemination, analysis, and visualization of multidimensional image data.

Lastly, since MPLSM, and all of the associated imaging modalities (MPE, SHG, FLIM, etc.) do not require a tissue biopsy to be fixed, sectioned, or stained, there is potential for MPLSM not only to serve a valuable research tool, but also as a diagnostic tool. The ability to image freshly harvested tissue for pathological evaluation could be of great clinical utility and could provide multiple sets of information (i.e., metabolic state, tumor cell phenotype, stromal composition, etc.) in a single imaged tumor volume. Moreover, the possibility of MPLSM as a clinical diagnostic tool must be considered. However, for MPLSM to be a clinical diagnostic tool, the technique needs to improve in both its depth penetration and the mode through which it is delivered. Adaptive-Optics based multiphoton (Marsh et al., 2003) has potential to greatly increase the depth penetration of MPLSM by the use of optics that can change their wavefront in response to changes in refractive index in tissue. However, there is not yet a practical implementation for MPLSM. Nonetheless, in the future, MPLSM does have the potential to be applied *in vivo* as a diagnostic tool through multiphoton fluorescence endoscopy (Bird & Gu, 2002a, 2002b, 2003; Jung & Schnitzer, 2003; Flusberg et al., 2005). As such it is feasible that MPLSM has the potential to be a real-time diagnostic tool for early cancer detection and possibly treatment.

Acknowledgments

The authors thank Dr. John White for his helpful comments and guidance regarding this work. This work was supported by grants from the DOD-CDMRP/BCRP (W81XWH-04-1-042) to P.P.P., the S.G. Komen Foundation (BCTR02-1841) and NIH (CA076537) to P.J.K. and NIH NIBIB (R01-EB000184) to K.W.E.

References

Abramoff MD, Magelhaes PJ, Ram SJ. Image processing with ImageJ. Biophoton Int. 2004; 11(7):36–42.

Ada-Nguema AS, Xenias H, Sheetz MP, Keely PJ. The small GTPase R-Ras regulates organization of actin and drives membrane protrusions through the activity of PLC{epsilon}. J Cell Sci. 2006; 119(Pt 7):1307–1319. [PubMed: 16537651]

Becker W, Bergmann A, Hink MA, Konig K, Benndorf K, Biskup C. Fluorescence lifetime imaging by time-correlated single-photon counting. Microsc Res Tech. 2004; 63(1):58–66. [PubMed: 14677134]

Bird D, Gu M. Fibre-optic two-photon scanning fluorescence microscopy. J Microsc. 2002a; 208(Pt 1): 35–48. [PubMed: 12366596]

Bird D, Gu M. Resolution improvement in two-photon fluorescence microscopy with a single-mode fiber. Appl Opt. 2002b; 41(10):1852–1857. [PubMed: 11936781]

Bird D, Gu M. Two-photon fluorescence endoscopy with a micro-optic scanning head. Opt Lett. 2003; 28(17):1552–1554. [PubMed: 12956376]

Bird DK, Eliceiri KW, Fan CH, White JG. Simultaneous two-photon spectral and lifetime fluorescence microscopy. Appl Opt. 2004; 43(27):5173–5182. [PubMed: 15473237]

Bird DK, Yan L, Vrotsos KM, Eliceiri KW, Vaughan EM, Keely PJ, White JG, Ramanujam N. Metabolic mapping of MCF10A human breast cells via multiphoton fluorescence lifetime imaging of the coenzyme NADH. Cancer Res. 2005; 65(19):8766–8773. [PubMed: 16204046]

Boyd NF, Dite GS, Stone J, Gunasekara A, English DR, McCredie MR, Giles GG, Tritchler D, Chiarelli A, Yaffe MJ, Hopper JL. Heritability of mammographic density, a risk factor for breast cancer. N Engl J Med. 2002; 347(12):886–894. [PubMed: 12239257]

Boyd NF, Lockwood GA, Byng JW, Tritchler DL, Yaffe MJ. Mammographic densities and breast cancer risk. Cancer Epidemiol Biomarkers Prev. 1998; 7(12):1133–1144. [PubMed: 9865433]

Boyd NF, Martin LJ, Stone J, Greenberg C, Minkin S, Yaffe MJ. Mammographic densities as a marker of human breast cancer risk and their use in chemoprevention. Curr Oncol Rep. 2001; 3(4):314–321. [PubMed: 11389815]

Brakenhoff GJ, van der Voort HT, van Spronsen EA, Linnemans WA, Nanninga N. Three-dimensional chromatin distribution in neuroblastoma nuclei shown by confocal scanning laser microscopy. Nature. 1985; 317(6039):748–749. [PubMed: 4058582]

Brown E, McKee T, diTomaso E, Pluen A, Seed B, Boucher Y, Jain RK. Dynamic imaging of collagen and its modulation in tumors in vivo using second-harmonic generation. Nat Med. 2003; 9(6):796–800. [PubMed: 12754503]

Brown EB, Campbell RB, Tsuzuki Y, Xu L, Carmeliet P, Fukumura D, Jain RK. *In vivo* measurement of gene expression, angiogenesis and physiological function in tumors using multiphoton laser scanning microscopy. Nat Med. 2001; 7(7):864–868. [PubMed: 11433354]

Campagnola PJ, Millard AC, Terasaki M, Hoppe PE, Malone CJ, Mohler WA. Three-dimensional high-resolution second-harmonic generation imaging of endogenous structural proteins in biological tissues. Biophys J. 2002; 82(1 Pt 1):493–508. [PubMed: 11751336]

Centonze VE, White JG. Multiphoton excitation provides optical sections from deeper within scattering specimens than confocal imaging. Biophys J. 1998; 75(4):2015–2024. [PubMed: 9746543]

Condeelis J, Singer RH, Segall JE. The great escape: When cancer cells hijack the genes for chemotaxis and motility. Annu Rev Cell Dev Biol. 2005; 21:695–718. [PubMed: 16212512]

Cox G, Kable E, Jones A, Fraser I, Manconi F, Gorrell MD. 3-dimensional imaging of collagen using second harmonic generation. J Struct Biol. 2003; 141(1):53–62. [PubMed: 12576020]

Cremazy FG, Manders EM, Bastiaens PI, Kramer G, Hager GL, van Munster EB, Verschure PJ, Gadella TJ Jr, van Driel R. Imaging *in situ* protein-DNA interactions in the cell nucleus using FRET-FLIM. Exp Cell Res. 2005; 309(2):390–396. [PubMed: 16040027]

DeMali KA, Burridge K. Coupling membrane protrusion and cell adhesion. J Cell Sci. 2003; 116(12): 2389–2397. [PubMed: 12766185]

Denk W, Strickler JH, Webb WW. Two-photon laser scanning fluorescence microscopy. Science. 1990; 248(4951):73–76. [PubMed: 2321027]

Diaspro, A., Sheppard, CJR. Two-photon excitation fluorescence microscopy. In: Diaspro, A., editor. Confocal and Two-Photon Microscopy: Foundations, Applications, and Advances. New York: Wiley-Liss, Inc; 2002. p. 39-73.

Elenbaas B, Spirio L, Koerner F, Fleming MD, Zimonjic DB, Donaher JL, Popescu NC, Hahn WC, Weinberg RA. Human breast cancer cells generated by oncogenic transformation of primary mammary epithelial cells. Genes Dev. 2001; 15(1):50–65. [PubMed: 11156605]

Eliceiri KW, Fan CH, Lyons GE, White JG. Analysis of histology specimens using lifetime multiphoton microscopy. J Biomed Opt. 2003; 8(3):376–380. [PubMed: 12880342]

Eliceiri KW, Rueden C. Tools for visualizing multidimensional images from living specimens. Photochem Photobiol. 2005; 81(5):1116–1122. [PubMed: 15807634]

Flusberg BA, Cocker ED, Piyawattanametha W, Jung JC, Cheung EL, Schnitzer MJ. Fiber-optic fluorescence imaging. Nat Methods. 2005; 2(12):941–950. [PubMed: 16299479]

French T, So PT, Weaver DJ Jr, Coelho-Sampaio T, Gratton E, Voss EW Jr, Carrero J. Two-photon fluorescence lifetime imaging microscopy of macrophage-mediated antigen processing. J Microsc. 1997; 185(Pt 3):339–353. [PubMed: 9134740]

Freund I, Deutsch M. Second-harmonic microscopy of biological tissue. Opt Lett. 1986; 11(2):94–96. [PubMed: 19730544]

Friedl P, Hegerfeldt Y, Tusch M. Collective cell migration in morphogenesis and cancer. Int J Dev Biol. 2004; 48(5–6):441–449. [PubMed: 15349818]

Friedl P, Wolf K. Tumour-cell invasion and migration: Diversity and escape mechanisms. Nat Rev Cancer. 2003; 3(5):362–374. [PubMed: 12724734]

Galeotti T, van Rossum GD, Mayer DH, Chance B. On the fluorescence of NAD(P)H in whole-cell preparations of tumours and normal tissues. Eur J Biochem. 1970; 17(3):485–496. [PubMed: 4395441]

Goldberg IG, Allan C, Burel JM, Creager D, Falconi A, Hochheiser H, Johnston J, Mellen J, Sorger PK, Swedlow JR. The Open Microscopy Environment (OME) Data Model and XML file: Open tools for informatics and quantitative analysis in biological imaging. Genome Biol. 2005; 6(5):R47. [PubMed: 15892875]

Guo YP, Martin LJ, Hanna W, Banerjee D, Miller N, Fishell E, Khokha R, Boyd NF. Growth factors and stromal matrix proteins associated with mammographic densities. Canc Epid Biomark Prev. 2001; 10(3):243–248.

Hagios C, Lochter A, Bissell MJ. Tissue architecture: The ultimate regulator of epithelial function? Philos Trans R Soc Lond B Biol Sci. 1998; 353(1370):857–870. [PubMed: 9684283]

Hanahan D, Weinberg RA. The hallmarks of cancer. Cell. 2000; 100(1):57–70. [PubMed: 10647931]

Harpur AG, Wouters FS, Bastiaens PI. Imaging FRET between spectrally similar GFP molecules in single cells. Nat Biotechnol. 2001; 19(2):167–169. [PubMed: 11175733]

Hegerfeldt Y, Tusch M, Brocker EB, Friedl P. Collective cell movement in primary melanoma explants: Plasticity of cell-cell interaction, {beta}1-integrin function, and migration strategies. Cancer Res. 2002; 62(7):2125–2130. [PubMed: 11929834]

Helmchen F, Denk W. New developments in multiphoton microscopy. Curr Opin Neurobiol. 2002; 12(5):593–601. [PubMed: 12367641]

Huang S, Heikal AA, Webb WW. Two-photon fluorescence spectroscopy and microscopy of NAD(P)H and flavoprotein. Biophys J. 2002; 82(5):2811–2825. [PubMed: 11964266]

Jacks T, Weinberg RA. Taking the study of cancer cell survival to a new dimension. Cell. 2002; 111(7): 923–925. [PubMed: 12507419]

Jaffe AB, Hall A. RHO GTPASES: Biochemistry and biology. Ann Rev Cell Dev Biol. 2005; 21(1): 247–269. [PubMed: 16212495]

Jain RK, Munn LL, Fukumura D. Dissecting tumour pathophysiology using intravital microscopy. Nat Rev Cancer. 2002; 2(4):266–276. [PubMed: 12001988]

Jung JC, Schnitzer MJ. Multiphoton endoscopy. Opt Lett. 2003; 28(11):902–904. [PubMed: 12816240]

Katz A, Savage HE, Schantz SP, McCormick SA, Alfano RR. Noninvasive native fluorescence imaging of head and neck tumors. Technol Cancer Res Treat. 2002; 1(1):9–15. [PubMed: 12614172]

Keely P, Fong A, Zutter M, Santoro S. Alteration of collagen-dependent adhesion, motility, and morphogenesis by the expression of antisense a2 integrin mRNA in mammary cells. J Cell Sci. 1995; 108:595–607. [PubMed: 7769004]

Keely PJ, Rusyn EV, Cox AD, Parise LV. R-Ras signals through specific integrin alpha cytoplasmic domains to promote migration and invasion of breast epithelial cells. J Cell Biol. 1999; 145(5): 1077–1088. [PubMed: 10352023]

Kirkpatrick ND, Zou C, Brewer MA, Brands WR, Drezek RA, Utzinger U. Endogenous fluorescence spectroscopy of cell suspensions for chemopreventive drug monitoring. Photochem Photobiol. 2005; 81(1):125–134. [PubMed: 15535738]

Lakowicz JR, Szmacinski H, Nowaczyk K, Berndt KW, Johnson M. Fluorescence lifetime imaging. Anal Biochem. 1992; 202(2):316–330. [PubMed: 1519759]

Lee KC, Siegel J, Webb SE, Leveque-Fort S, Cole MJ, Jones R, Dowling K, Lever MJ, French PM. Application of the stretched exponential function to fluorescence lifetime imaging. Biophys J. 2001; 81(3):1265–1274. [PubMed: 11509343]

Lin EY, Jones JG, Li P, Zhu L, Whitney KD, Muller WJ, Pollard JW. Progression to malignancy in the polyoma middle T oncoprotein mouse breast cancer model provides a reliable model for human diseases. Am J Pathol. 2003; 163(5):2113–2126. [PubMed: 14578209]

Lippincott-Schwartz J, Patterson GH. Development and use of fluorescent protein markers in living cells. Science. 2003; 300(5616):87–91. [PubMed: 12677058]

Lippincott-Schwartz J, Snapp E, Kenworthy A. Studying protein dynamics in living cells. Nat Rev Mol Cell Biol. 2001; 2(6):444–456. [PubMed: 11389468]

Marsh P, Burns D, Girkin J. Practical implementation of adaptive optics in multiphoton microscopy. Opt Exp. 2003; 11:1123–1130.

Mohler W, Millard AC, Campagnola PJ. Second harmonic generation imaging of endogenous structural proteins. Methods. 2003; 29(1):97–109. [PubMed: 12543075]

Muti P. The role of endogenous hormones in the etiology and prevention of breast cancer: The epidemiological evidence. Ann NY Acad Sci. 2004; 1028:273–282. [PubMed: 15650252]

Nazir, MZ., Eliceiri, KW. WiscScan: A Software Defined Laser-Scanning Microscope. 2008. Personal Communication

Palmer GM, Keely PJ, Breslin TM, Ramanujam N. Autofluorescence spectroscopy of normal and malignant human breast cell lines. Photochem Photobiol. 2003; 78(5):462–469. [PubMed: 14653577]

Parsons M, Monypenny J, Ameer-Beg SM, Millard TH, Machesky LM, Peter M, Keppler MD, Schiavo G, Watson R, Chernoff J, Zicha D, Vojnovic B, Ng T. Spatially distinct binding of Cdc42 to PAK1 and N-WASP in breast carcinoma cells. Mol Cell Biol. 2005; 25(5):1680–1695. [PubMed: 15713627]

Paszek MJ, Zahir N, Johnson KR, Lakins JN, Rozenberg GI, Gefen A, Reinhart-King CA, Margulies SS, Dembo M, Boettiger D, Hammer DA, Weaver VM. Tensional homeostasis and the malignant phenotype. Cancer Cell. 2005; 8(3):241–254. [PubMed: 16169468]

Patterson GH, Knobel SM, Arkhammar P, Thastrup O, Piston DW. Separation of the glucose-stimulated cytoplasmic and mitochondrial NAD(P)H responses in pancreatic islet beta cells. Proc Natl Acad Sci USA. 2000; 97(10):5203–5207. [PubMed: 10792038]

Peter M, Ameer-Beg SM. Imaging molecular interactions by multiphoton FLIM. Biol Cell. 2004; 96(3):231–236. [PubMed: 15182705]

Peter M, Ameer-Beg SM, Hughes MK, Keppler MD, Prag S, Marsh M, Vojnovic B, Ng T. Multiphoton-FLIM quantification of the EGFP-mRFP1 FRET pair for localization of membrane receptor-kinase interactions. Biophys J. 2005; 88(2):1224–1237. [PubMed: 15531633]

Pitts JD, Sloboda RD, Dragnev KH, Dmitrovsky E, Mycek MA. Autofluorescence characteristics of immortalized and carcinogen-transformed human bronchial epithelial cells. J Biomed Opt. 2001; 6(1):31–40. [PubMed: 11178578]

Plotnikov SV, Millard AC, Campagnola PJ, Mohler WA. Characterization of the myosin-based source for second-harmonic generation from muscle sarcomeres. Biophys J. 2006; 90(2):693–703. [PubMed: 16258040]

Poteryaev D, Squirrell JM, Campbell JM, White JG, Spang A. Involvement of the actin cytoskeleton and homotypic membrane fusion in ER dynamics in caenorhabditis elegans. Mol Biol Cell. 2005; 16(5):2139–2153. [PubMed: 15716356]

Pradhan A, Pal P, Durocher G, Villeneuve L, Balassy A, Babai F, Gaboury L, Blanchard L. Steady state and time-resolved fluorescence properties of metastatic and non-metastatic malignant cells from different species. J Photochem Photobiol B. 1995; 31(3):101–112. [PubMed: 8583278]

Provenzano PP, Eliceiri KW, Campbell JM, Inman DR, White JG, Keely PJ. Collagen reorganization at the tumor-stromal interface facilitates local invasion. BMC Med. 2006; 4(1):38. [PubMed: 17190588]

Ramanujam N. Fluorescence spectroscopy of neoplastic and non-neoplastic tissues. Neoplasia. 2000; 2(1–2):89–117. [PubMed: 10933071]

Rangarajan A, Hong SJ, Gifford A, Weinberg RA. Species- and cell type-specific requirements for cellular transformation. Cancer Cell. 2004; 6(2):171–183. [PubMed: 15324700]

Robu VG, Pfeiffer ES, Robia SL, Balijepalli RC, Pi Y, Kamp TJ, Walker JW. Localization of functional endothelin receptor signaling complexes in cardiac transverse tubules. J Biol Chem. 2003; 278(48):48154–48161. [PubMed: 12972433]

Ronnov-Jessen L, Petersen OW, Koteliansky VE, Bissell MJ. The origin of the myofibroblasts in breast cancer. Recapitulation of tumor environment in culture unravels diversity and implicates converted fibroblasts and recruited smooth muscle cells. J Clin Invest. 1995; 95(2):859–873. [PubMed: 7532191]

Rueden C, Eliceiri KW, White JG. VisBio: A computational tool for visualization of multidimensional biological image data. Traffic. 2004; 5(6):411–417. [PubMed: 15117315]

Sahai E, Wyckoff J, Philippar U, Segall JE, Gertler F, Condeelis J. Simultaneous imaging of GFP, CFP and collagen in tumors *in vivo* using multiphoton microscopy. BMC Biotechnol. 2005; 5:14. [PubMed: 15910685]

Sato N, Maehara N, Goggins M. Gene expression profiling of tumor-stromal interactions between pancreatic cancer cells and stromal fibroblasts. Cancer Res. 2004; 64(19):6950–6956. [PubMed: 15466186]

Shen YR. Surface properties probed by second-harmonic and sum-frequency generation. Nature. 1989; 337(9):519–525.

Skala MC, Squirrell JM, Vrotsos KM, Eickhoff JC, Gendron-Fitzpatrick A, Eliceiri KW, Ramanujam N. Multiphoton microscopy of endogenous fluorescence differentiates normal, precancerous, and cancerous squamous epithelial tissues. Cancer Res. 2005; 65(4):1180–1186. [PubMed: 15735001]

Squirrell JM, Eggers ZT, Luedke N, Saari B, Grimson A, Lyons GE, Anderson P, White JG. CAR-1, a protein that localizes with the mRNA decapping component DCAP-1, is required for cytokinesis and ER organization in caenorhabditis elegans embryos. Mol Biol Cell. 2006; 17(1):336–344. [PubMed: 16267265]

Squirrell JM, Wokosin DL, White JG, Bavister BD. Long-term two-photon fluorescence imaging of mammalian embryos without compromising viability. Nat Biotechnol. 1999; 17(8):763–767. [PubMed: 10429240]

Stoller P, Kim BM, Rubenchik AM, Reiser KM, Da Silva LB. Polarization-dependent optical second-harmonic imaging of a rat-tail tendon. J Biomed Opt. 2002; 7(2):205–214. [PubMed: 11966305]

Strome S, Powers J, Dunn M, Reese K, Malone CJ, White J, Seydoux G, Saxton W. Spindle dynamics and the role of {gamma}-tubulin in early caenorhabditis elegans embryos. Mol Biol Cell. 2001; 12(6):1751–1764. [PubMed: 11408582]

Tadrous PJ, Siegel J, French PM, Shousha S, Lalani el N, Stamp GW. Fluorescence lifetime imaging of unstained tissues: Early results in human breast cancer. J Pathol. 2003; 199(3):309–317. [PubMed: 12579532]

Tlsty TD, Hein PW. Know thy neighbor: Stromal cells can contribute oncogenic signals. Curr Opin Genet Dev. 2001; 11(1):54–59. [PubMed: 11163151]

van Munster EB, Gadella TW. Fluorescence lifetime imaging microscopy (FLIM). Adv Biochem Eng Biotechnol. 2005; 95:143–175. [PubMed: 16080268]

Verveer PJ, Wouters FS, Reynolds AR, Bastiaens PI. Quantitative imaging of lateral ErbB1 receptor signal propagation in the plasma membrane. Science. 2000; 290(5496):1567–1570. [PubMed: 11090353]

Wang W, Goswami S, Lapidus K, Wells AL, Wyckoff JB, Sahai E, Singer RH, Segall JE, Condeelis JS. Identification and testing of a gene expression signature of invasive carcinoma cells within primary mammary tumors. Cancer Res. 2004; 64(23):8585–8594. [PubMed: 15574765]

Wang W, Goswami S, Sahai E, Wyckoff JB, Segall JE, Condeelis JS. Tumor cells caught in the act of invading: Their strategy for enhanced cell motility. Trends Cell Biol. 2005; 15(3):138–145. [PubMed: 15752977]

Wang W, Wyckoff JB, Frohlich VC, Oleynikov Y, Huttelmaier S, Zavadil J, Cermak L, Bottinger EP, Singer RH, White JG, Segall JE, Condeelis JS. Single cell behavior in metastatic primary mammary tumors correlated with gene expression patterns revealed by molecular profiling. Cancer Res. 2002; 62(21):6278–6288. [PubMed: 12414658]

West RB, Nuyten DS, Subramanian S, Nielsen TO, Corless CL, Rubin BP, Montgomery K, Zhu S, Patel R, Hernandez-Boussard T, Goldblum JR, Brown PO, van de Vijver M, van de Rijn M. Determination of stromal signatures in breast carcinoma. PLoS Biol. 2005; 3(6):e187. [PubMed: 15869330]

White JG, Amos WB, Fordham M. An evaluation of confocal versus conventional imaging of biological structures by fluorescence light microscopy. J Cell Biol. 1987; 105(1):41–48. [PubMed: 3112165]

Williams RM, Zipfel WR, Webb WW. Interpreting second-harmonic generation images of collagen I fibrils. Biophys J. 2005; 88(2):1377–1386. [PubMed: 15533922]

Wokosin DL, Squirrell JM, Eliceiri KE, White JG. An optical workstation with concurrent, independent multiphoton imaging and experimental laser microbeam capabilities. Rev Sci Instrum. 2003; 74(1):193–201. [PubMed: 18607511]

Wozniak MA, Desai R, Solski PA, Der CJ, Keely PJ. ROCK-generated contractility regulates breast epithelial cell differentiation in response to the physical properties of a three-dimensional collagen matrix. J Cell Biol. 2003; 163(3):583–595. [PubMed: 14610060]

Wozniak MA, Kwong L, Chodniewicz D, Klemke RL, Keely PJ. R-Ras controls membrane protrusion and cell migration through the spatial regulation of Rac and Rho. Mol Biol Cell. 2005; 16(1):84–96. [PubMed: 15525681]

Yan L, Rueden CT, White JG, Eliceiri KW. Applications of combined spectral lifetime microscopy for biology. Biotechniques. 2006; 41(3):249, 251, 253. passim. [PubMed: 16989084]

Zhang J, Campbell RE, Ting AY, Tsien RY. Creating new fluorescent probes for cell biology. Nat Rev Mol Cell Biol. 2002; 3(12):906–918. [PubMed: 12461557]

Zipfel WR, Williams RM, Christie R, Nikitin AY, Hyman BT, Webb WW. Live tissue intrinsic emission microscopy using multiphoton-excited native fluorescence and second harmonic generation. Proc Natl Acad Sci USA. 2003a; 100(12):7075–7080. [PubMed: 12756303]

Zipfel WR, Williams RM, Webb WW. Nonlinear magic: Multiphoton microscopy in the biosciences. Nat Biotechnol. 2003b; 21(11):1369–1377. [PubMed: 14595365]

Zoumi A, Yeh A, Tromberg BJ. Imaging cells and extracellular matrix *in vivo* by using second-harmonic generation and two-photon excited fluorescence. Proc Natl Acad Sci USA. 2002; 99(17): 11014–11019. [PubMed: 12177437]

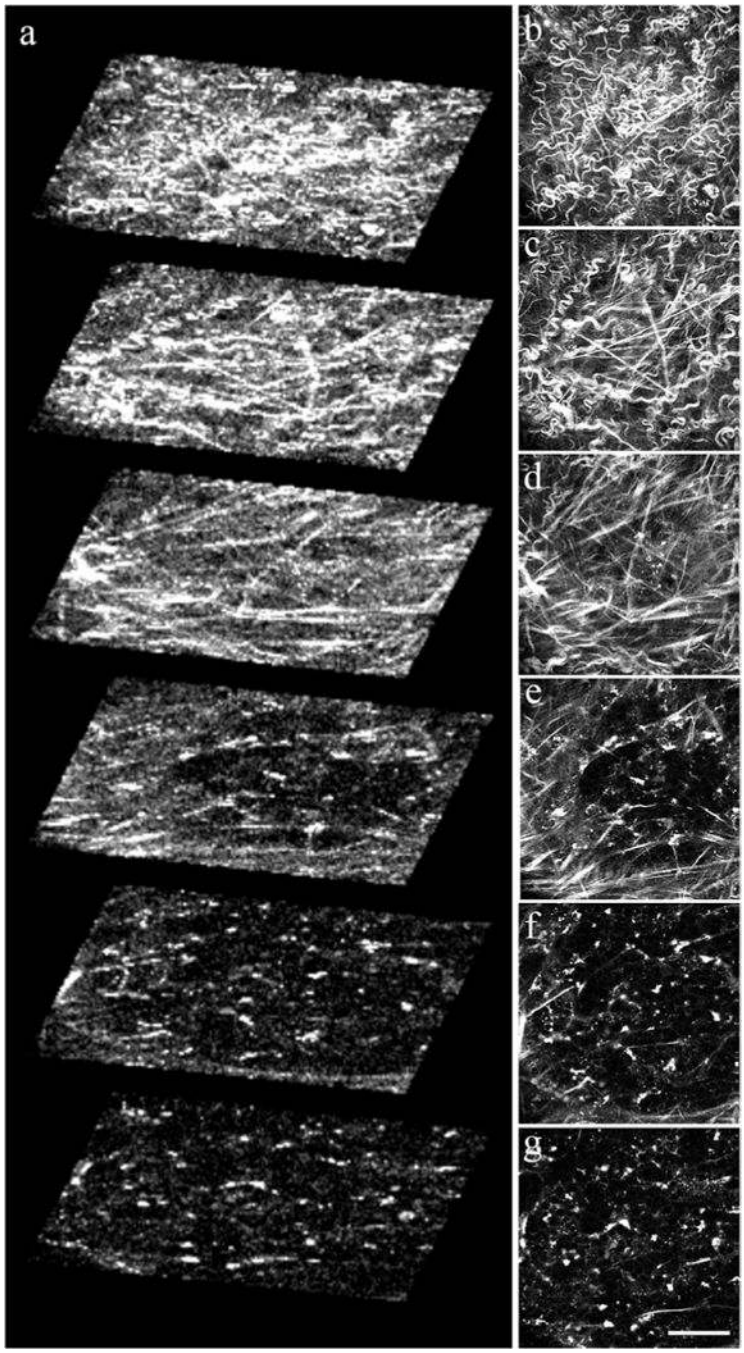

Figure 1.

Live mammary tumor. Combined MPE and SHG at λ_{ex} = 890 nm facilitates imaging of intact live mammary tumor tissue. **a:** Six planes of a 30-plane z-stack acquired every 10 μm (i.e., 300 μm total stack) into the tumor that was rendered and oriented with VisBio. **b–g:** The flat images for each corresponding imaging plane. Combined, **a–g** clearly show variations in endogenous cellular fluorescence as well as collagen surrounding and within the tumor validating the ability to image deep into live tissue and obtain meaningful information. Bar = 50 μm.

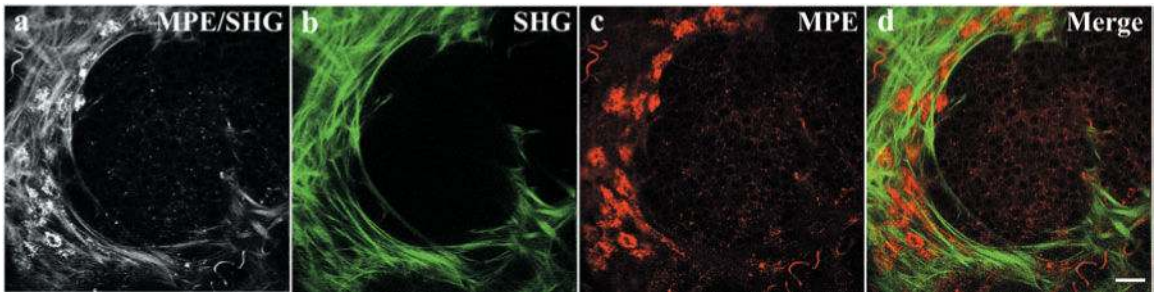

Figure 2.

MPE and SHG signal separation in live tumor. Since MPE excitation follows classical energy loss behavior while SHG signals are conserved, filtering techniques can be employed to separate the two signals following excitation with the same wavelength. Following excitation of live mammary tumor tissue with a wavelength (λ_{ex} = 890 nm) that elicits both endogenous cellular fluorescence (of FAD) and SHG (**a**), the resultant emissions were separated using a 445 nm narrow band pass filter for SHG (**b**: pseudocolored green) and a 464 nm (cut-on) long pass filter for MPE (**c**: pseudocolored red). This approach allows clear visualization of the collagenous stroma (**b**) as well as stromal cells, localized within the collagen matrix, and tumor cells (**c**), while merging the two pseudocolored signals (**d**) helps reveal cell matrix interactions associated with the tumor-stromal interface. As such, the use of combined MPE/SHG has the potential to help identify and differentiate additional features that are not readily obtained with more traditional fluorescent microscopy techniques. Bar = 25 μm.

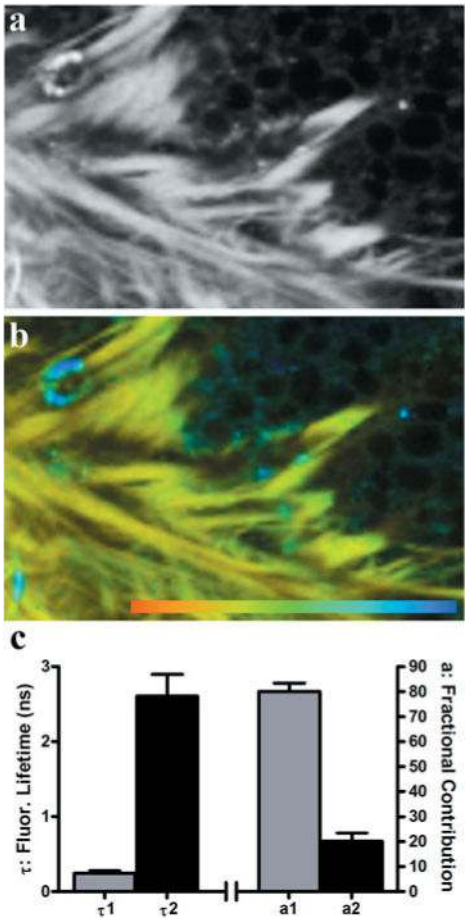

Figure 3.

Multiphoton FLIM of live mammary tumor. Following excitation at 890 nm, lifetime data were collected for 60 s using the Optical Work Station (described in the Instrumentation section) and displayed as (**a**) intensity or (**b**) color-mapped lifetimes (color bar 0 to 1.2 ns; red to blue) for a two-term exponential model (see equation (3)). The color mapping represents the weighted average of the short and long components: $\tau_m = (a_1\tau_1 + a_2\tau_2)/(a_1 + a_2)$, although the relative contribution of each component for cells in the tumor is shown in **c**. Additionally, due to the fact that signals from collagen principally arise from the conserved SHG polarization, the resulting signal has a theoretical lifetime of zero, which is supported by the fact that the majority of the collagen signal closely follows the instrumental response function.

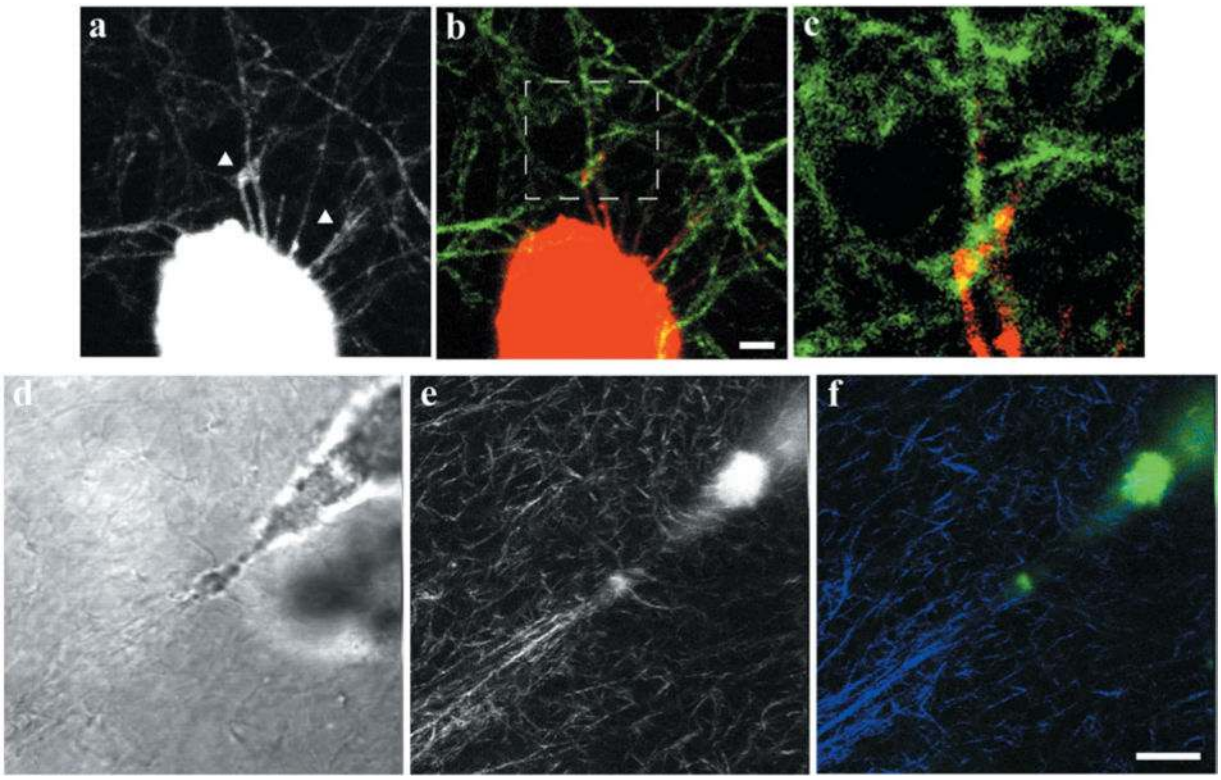

Figure 4.

Invasive breast carcinoma cells in 3D matrices. Highly invasive and migratory MDA-MB-231 breast carcinoma cells were cultured within reconstituted 3D collagen matrices to further examine the utility of combined MPE/SHG to probe the cell-matrix interaction. After 3 h in collagen gels (**a**–**c**), MDA-MB-231 cells expressing GFP-Vinculin form 3D matrix adhesions by presenting filopodia that interact with collagen fibers (arrows in **a**). As is shown in **b**, this interaction can be highlighted by separating the SHG signal (445 nm narrow band pass filter; green pseudocolor) and the GFP signal (480–550 nm band pass filter; red pseudocolor), while **c** is a magnified region (dashed box) of **b** clearly demonstrating vinculin positive filopodia interacting with collagen fibers (colocalization = yellow). After 24 h in 3D collage matrices (**d**: transmitted light), MDA-MB-231(GFP-vinculin) cells have aligned collagen fibers with vinculin localization at the cell-matrix interface (**e**, **f**: GFP = green pseudocolor; SHG blue pseudocolor). Hence, simultaneous imaging of cellular processes and matrix organization and structure with combined MPE/SHG not only facilitates imaging of nonnative and endogenous signals *in vivo*, but also provides a robust tool to study tumor-stromal interactions in live unfixed, unstained, nonsectioned) cells *in vitro*, which can further our understanding of the *in vivo* condition. Bar (**a**–**c**) = 10 μm; bar (**d**–**f**) = 25 μm.

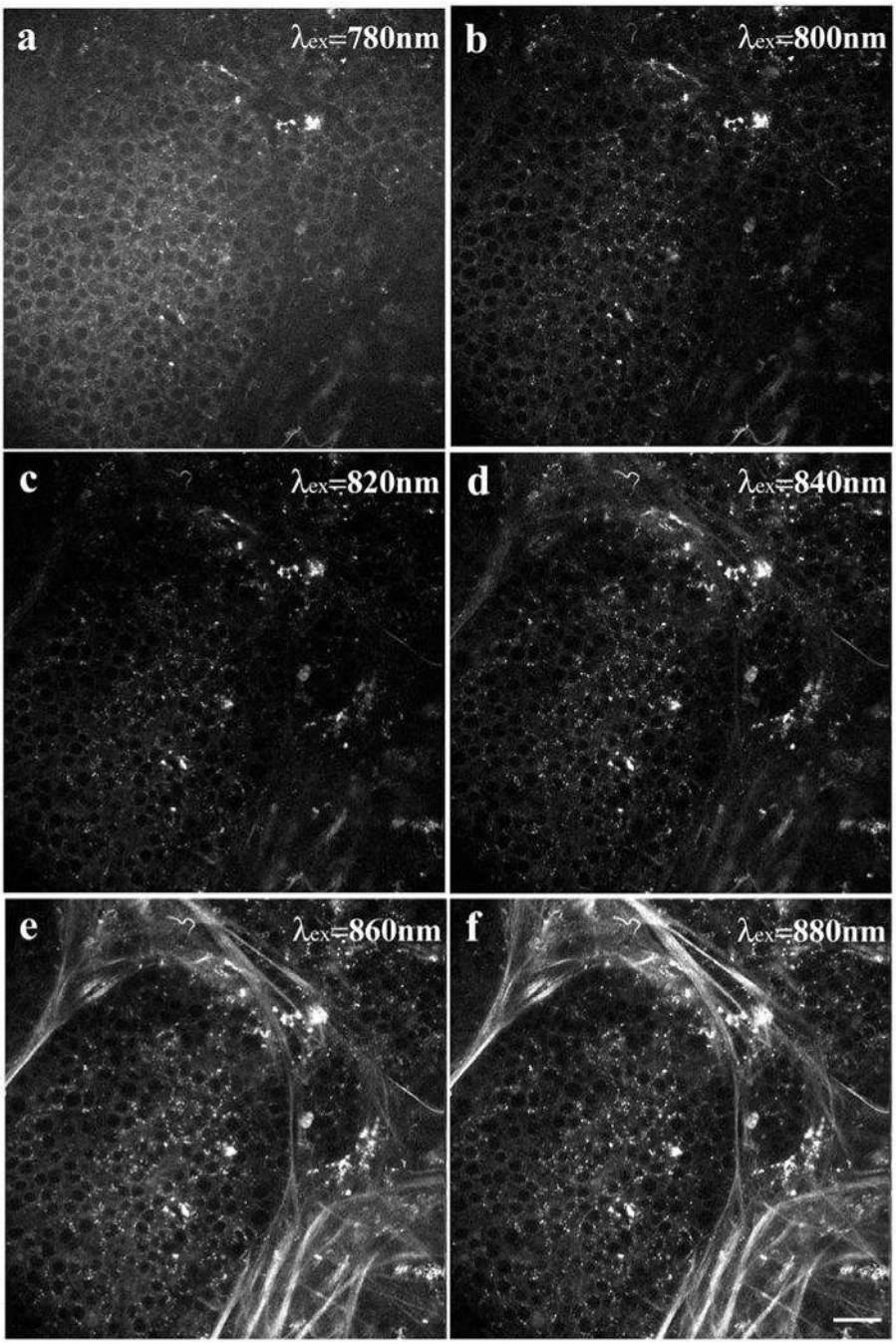

Figure 5.

Changes in breast tumor cell and matrix signals as a function of excitation wavelength. By increasing the excitation wavelength from 780 to 880 nm in 20 nm increments, changes in the intensity and localization of endogenous fluorescence as well the emergence of collagen SHG is detectable. At λ_{ex} = 780 nm (**a**), a two-photon wavelength that excites NADH, the cytoplasm of the tumor cells display a high degree of autofluorescence, which decreases as the excitation wavelength is increased (**b–d**). Additionally, minimal SHG signal from collagen is detectable below λ_{ex} = 860 nm. At λ_{ex} = 860 nm (**e**) and 880 nm (**f**), two-photon

wavelengths that excite FAD and produce collagen SHG, strong autofluorescent signal and clear collagen SHG signals are present. The strong signal at λ_{ex} = 780 nm, which decreases until λ_{ex} = 860 nm likely indicates emission from the endogenous fluorophore NADH at 780 nm that decreases and transitions to endogenous fluorescence from FAD as the excitation wavelength approaches 900 nm. Hence, MPLSM facilitates the ability to image two important endogenous fluorophores, NADH and FAD, as well as fibrillar collagen, allowing visualization of breast tumor cell behavior and for detecting and studying changes in tumor cell metabolism. Bar = 25 μm.

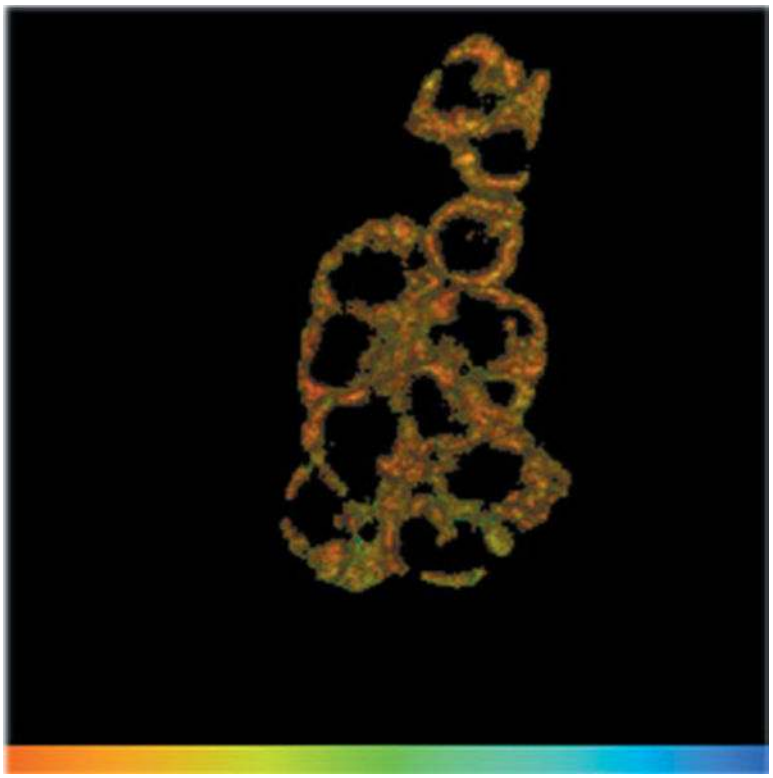

Figure 6.

Fluorescent lifetime of NADH in T47D breast carcinoma cells. TPE at 740 nm elicits endogenous fluorescence of NADH, with a fluorescence lifetime that is independent of NADH concentration. As such, imaging fluorescence intensity with MPE and fluorescence lifetime with FLIM facilitate direct monitoring of normal and tumor cell metabolic enzyme amount and state in key processes such as tumorigenesis and metastasis, as well as response to antitumor therapeutics. Color mapping represents the weighted average of the short and long components: $\tau_m = (a_1\tau_1 + a_2\tau_2)/(a_1 + a_2)$; color bar = 0.4 to 3 ns, red to blue.

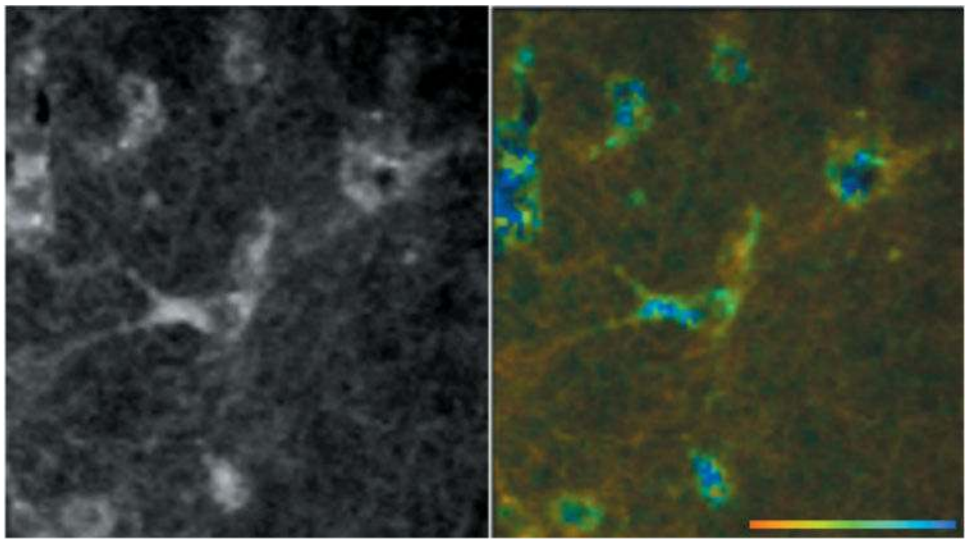

Figure 7.

Fluorescent lifetime of MDA-MB-231 breast carcinoma cells in 3D. 890 nm excitation of MDA-MB-231 breast carcinoma cells in 3D collagen gels. The color map represents the weighted average of the two-term model components [$\tau_m = (a_1\tau_1 + a_2\tau_2)/(a_1 + a_2)$] and validates the ability to detect changes in cellular lifetime of highly invasive breast carcinoma cells within a 3D culture environment. Color bar = 100 to 800 ps, red to blue.

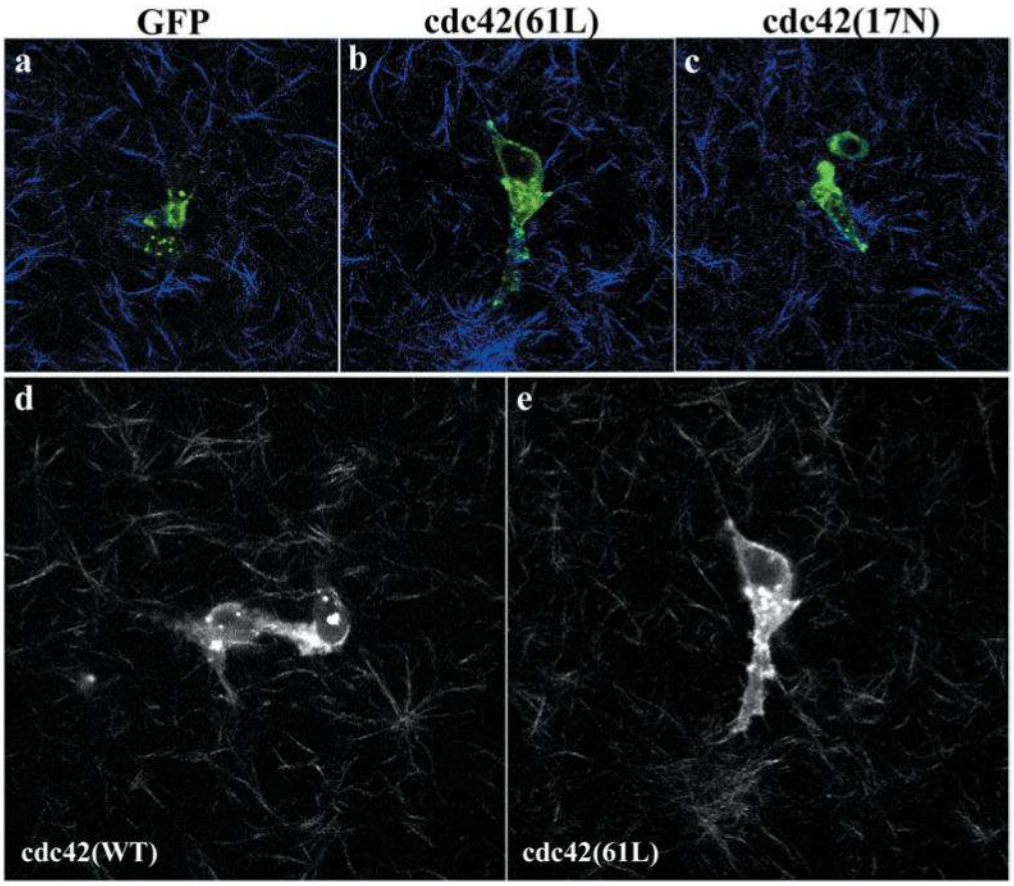

Figure 8.

Combined MPE/SHG of GFP-cdc42 in MDA-MB-231 cells within 3D collagen matrices. Live cells within type I collagen gels were imaged with combined MPE/SHG at λ_{ex} = 890 nm. After 6 h within 3D collagen gels, differences in cell morphology and the cell matrix interaction could be detected as a function of cdc42 state. Cells expressing constitutively active cdc42 (**b**) were more spread and presented more cell protrusions than both control GFP cells (**a**) and dominant negative expressing cells (**c**). Additionally overexpression of wild type cdc42 resulted in cell protrusion (**d**), but was not as spread as cells expressing constitutively active cdc42 (**e**). Moreover, separation of the GFP signal (480–550 nm band pass filter; green pseudocolor) from SHG (445 narrow band pass filter, blue pseudocolor) reveals increased cell matrix attachments in cdc42(61L) cells with cdc42 localized to cell protrusions that are interacting with the collagen matrix.

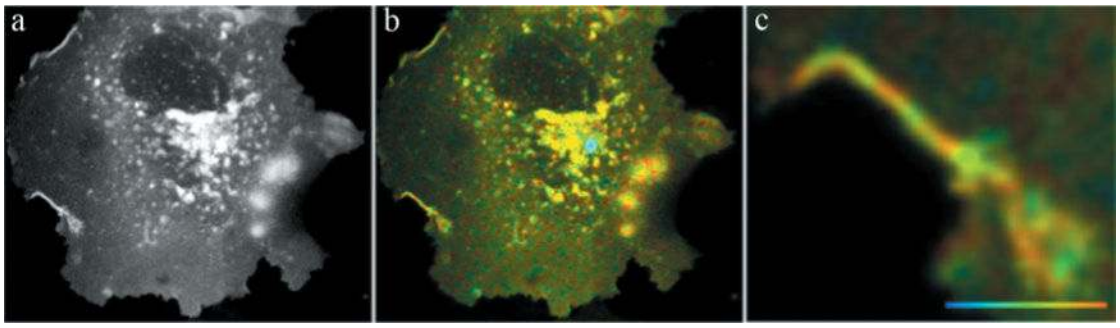

Figure 9.

Fluorescent lifetime imaging of a GFP-tagged molecule elucidates novel subdomains within the plasma membrane. GFP fused to constitutively active R-Ras (GFP-R-Ras(38V)) was transfected into Cos 7 cells and imaged by MPLSM: (**a**) intensity image and (**b**) color map of the FLIM of GFP-R-ras(38V) mapped from 1500 to 2500 ns; blue to red. (**c**) Blow up of plasma membrane region shown in **b**. Note that GFP-R-Ras(38V) localizes to active regions of the plasma membrane, which appear uniform in intensity via MPE in **a**, but map to distinct lifetime domains in **b** and **c**. FLIM was collected at 900 nm utilizing a 60× plan apo (Nikon) lens utilizing a lab-built MPLSM as described in Bird et al. (2004, 2005).

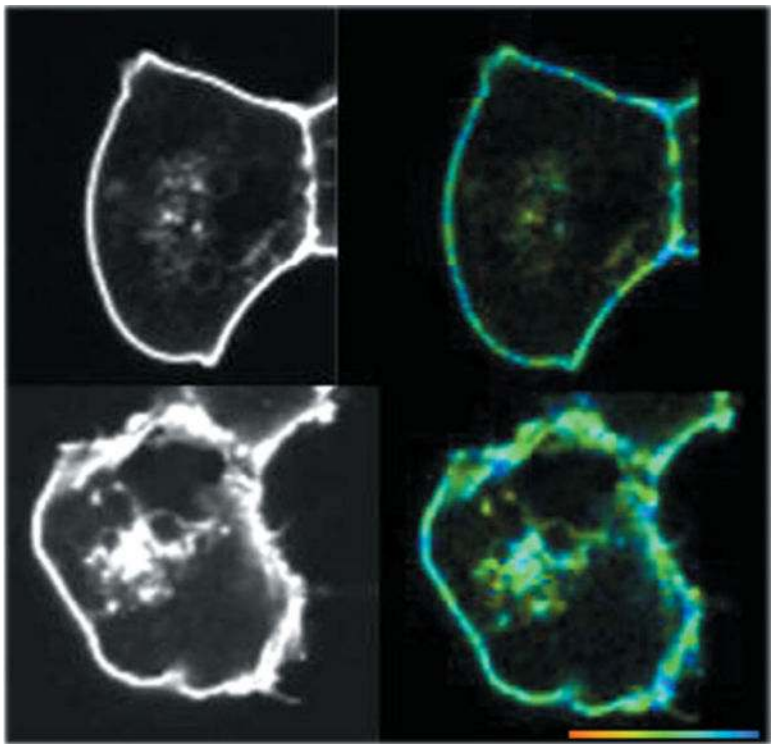

Figure 10.

FLIM of a lipophilic fluorescent molecule, filipin, reveals subdomains within the plasma membrane. Cos-7 cells were incubated in 50 μM of the cholesterol-binding fluorophore filipin for 30 min in order to detect microdomains of high cholesterol within the plasma membrane. Multiphoton excitation images of two exemplar cells are shown on the left. Color mapped (7 to 17 ns; red to blue) images representing the fluorescence lifetime of filipin were generated (right panels). The lifetime of this fluorophore was uncharacteristically long (>16 ns) throughout the entire membrane; however, there are subregions with distinguishable lifetimes, which map as distinct colors in discrete plasma membrane domains that are not detectable with standard multiphoton microscopy. FLIM was collected at 900 nm utilizing a 60× plan apo (Nikon) lens utilizing a lab-built MPLSM as described in Bird et al. (2004, 2005).

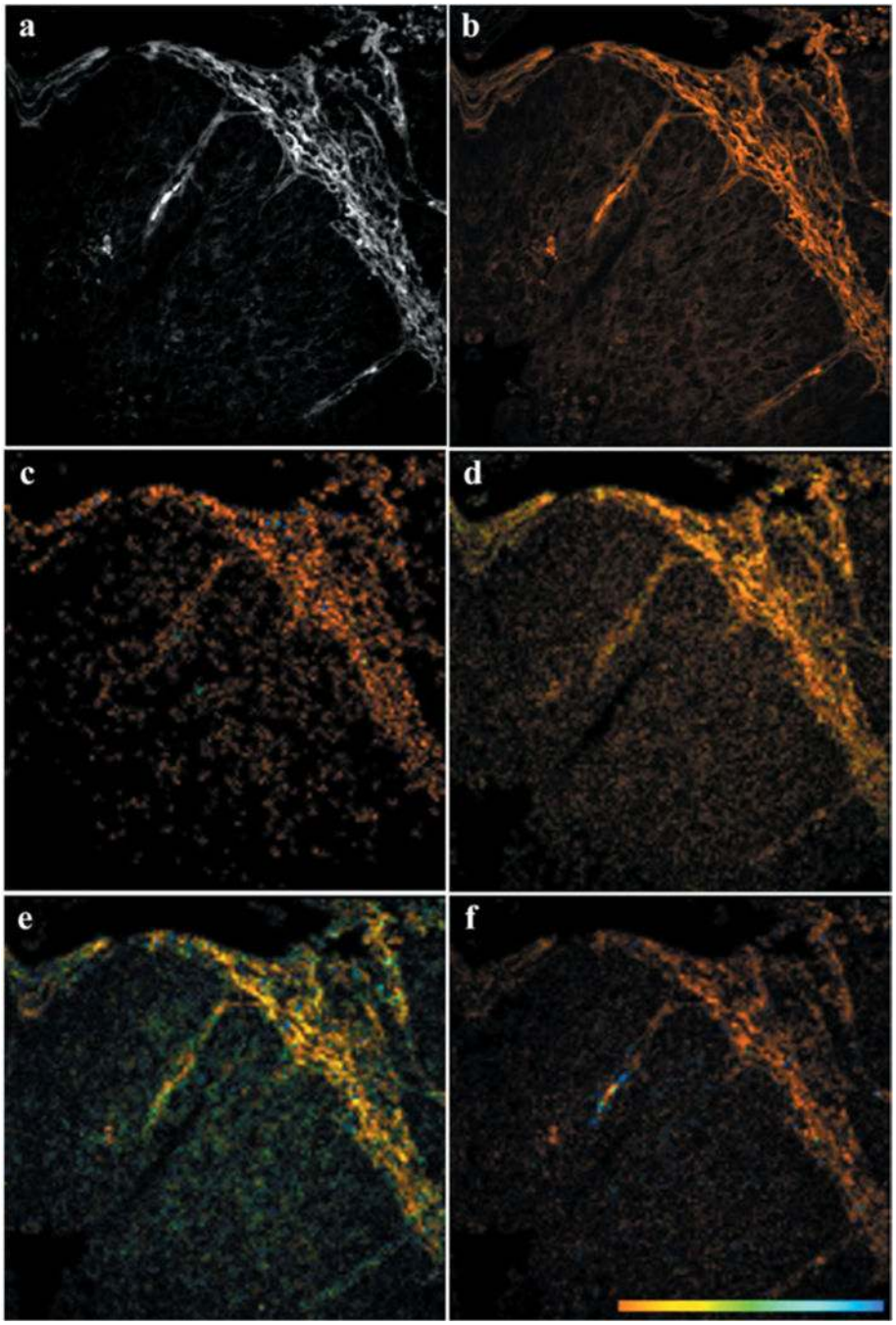

Figure 11.

SLIM analysis of tumor sections. Utilizing a recently developed MPLSM system (Yan et al., 2006) in the Laboratory for Optical and Computational Instrumentation, spectral lifetime data were obtained from hematoxylin and eosin stained polyoma middle-T mammary tumor sections. The emission spectra were separated into 10 nm components over 16 channels: (**a**) intensity image, (**b**) total FLIM signaling, and (**c–f**) the 510, 520, 530, and 540 nm emission components of the emission spectrum, respectively. Color mapping represents the weighted average of the two-term model components [$\tau_m = (a_1\tau_1 + a_2\tau_2)/(a_1 + a_2)$] with the color bar

extending from 0 to 5 ns; red to blue. Of particular note is the observation that the total signal appears largely as background (**b**), yet the 530 nm emission component (**e**) reveals a low lifetime for the stroma (yellow) and a longer lifetime for the tumor cells (mostly green and blue) indicating that narrowing the detection spectra range while removing adjacent spectral components, that are most likely contributing significant noise, allows imaging and analysis of otherwise masked information.